

Branching Fraction and CP Asymmetry Measurements in Inclusive $B \rightarrow X_s \ell^+ \ell^-$ and $B \rightarrow X_s \gamma$ Decays from $BABAR$

G. Eigen

representing the $BABAR$ collaboration

Department of Physics, University of Bergen, Allegaten 55, N-5007 Bergen, Norway

Abstract

We present an update on total and partial branching fractions and on CP asymmetries in the semi-inclusive decay $B \rightarrow X_s \ell^+ \ell^-$. Further, we summarize our results on branching fractions and CP asymmetries for semi-inclusive and fully-inclusive $B \rightarrow X_s \gamma$ decays. We present the first result on the CP asymmetry difference of charged and neutral $B \rightarrow X_s \gamma$ decays yielding the first constraint on the ratio of Wilson coefficients $Im(C_8^{\text{eff}}/C_7^{\text{eff}})$.

Keywords:

1. Introduction

The decays $B \rightarrow X_{s,d} \gamma$ and $B \rightarrow X_{s,d} \ell^+ \ell^-$ are flavor-changing neutral current (FCNC) processes that are forbidden in the Standard Model (SM) at tree level. However, they can proceed via penguin loops and box diagrams. Figure 1 shows the lowest-order diagrams for both processes. The effective Hamiltonian factorizes short-distance effects represented by perturbatively-calculable Wilson coefficients (C_i) [1, 2] from long-distance effects specified by four-quark operators (O_i):

$$H_{\text{eff}} = \frac{G_F}{4\pi} \sum_i V_{xb}^* V_{xs,d} C_i(\mu) O_i. \quad (1)$$

Here, G_F is the Fermi constant, V_{xb}^* and $V_{xs,d}$ are CKM elements ($x = u, c, t$) and μ is the renormalization scale. The operators have to be calculated using non-perturbative methods, such as the heavy quark expansion [3, 4, 5, 6]. In $B \rightarrow X_s \gamma$, the dominant contribution arises from the magnetic dipole operator O_7 with a top quark in the loop. Thus, the branching fraction depends on the Wilson coefficient $C_7^{\text{eff}} = -0.304$ (NNLL) [7, 8]. Via operator mixing, the color-magnetic dipole operator O_8 contributes in higher order with $C_8^{\text{eff}} = -0.167$ (NNLL) [7, 8]. In $B \rightarrow X_s \ell^+ \ell^-$, the weak penguin

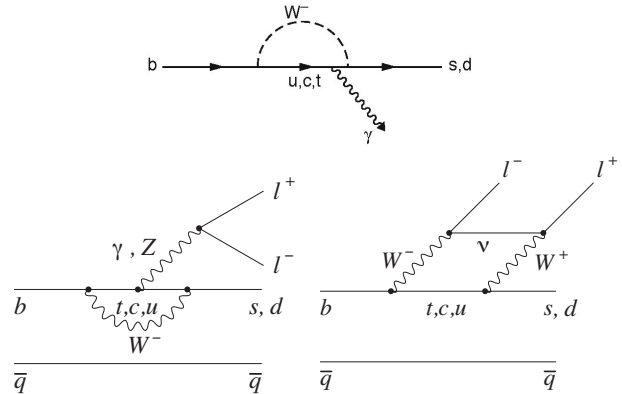


Figure 1: Lowest-order diagrams for $B \rightarrow X_{s,d} \gamma$ (top) and $B \rightarrow X_{s,d} \ell^+ \ell^-$ (bottom).

and box diagrams contribute in addition. The vector part is represented by operator O_9 with Wilson coefficient $C_9^{\text{eff}} = 4.211$ (NNLL) [7, 8] while the axial-vector part is specified by operator O_{10} with Wilson coefficient $C_{10}^{\text{eff}} = -4.103$ (NNLL) [7, 8]. Again, the top quark in the loop yields the most dominant contribution. New physics adds penguin and box diagrams with new particles modifying the SM values of the Wilson coefficients.

cients. In addition, scalar and pseudoscalar couplings may contribute introducing new Wilson coefficients C_S and C_P . Figure 2 shows examples of new physics processes involving a charged Higgs, a chargino and neutralinos [9, 10, 11, 12, 13, 14, 15]. These rare decays probe new physics at a scale of a few TeV.

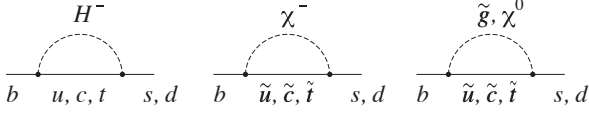


Figure 2: New physics processes with a charged Higgs bosons (left), a chargino plus up-type squarks (middle) and neutralinos plus down-type squarks (right).

2. Study of $B \rightarrow X_s \ell^+ \ell^-$

Using a semi-inclusive approach, we have updated the partial and total branching fraction measurements of $B \rightarrow X_s \ell^+ \ell^-$ modes with the full BABAR data sample of $471 \times 10^6 B\bar{B}$ events. We also perform the first measurement of direct CP asymmetry. For measuring partial and total branching fractions, we reconstruct 20 exclusive final states listed in Table 1. After accounting for K_L^0 modes, $K_S^0 \rightarrow \pi^0 \pi^0$ and π^0 Dalitz decays, they represent 70% of the inclusive rate for hadronic masses $m_{X_s} < 1.8$ GeV. Using JETSET fragmentation and theory predictions, we extrapolate for the missing modes and those with $m_{X_s} > 1.8$ GeV. We impose requirements on the beam-energy-substituted mass $m_{ES} = \sqrt{E_{CM}^2 - p_B^{*2}} > 5.225$ GeV and on the energy difference -0.1 (0.05) $< \Delta E = E_B^* - E_{CM}/2 < 0.05$ for $X_s e^+ e^-$ ($X_s \mu^+ \mu^-$) modes where E_B^* and p_B^* are B momentum and B energy in the center-of-mass (CM) frame and E_{CM} is the total CM energy. We use no tagging of the \bar{B} decay.

To suppress $e^+ e^- \rightarrow q\bar{q}$ ($q = u, d, s, c$) events and $B\bar{B}$ combinatorial background, we define boosted decision trees (BDT) for each q^2 bin in $e^+ e^-$ and $\mu^+ \mu^-$ separately (see Table 2). From these BDTs, we determine a likelihood ratio (L_R) to separate signal from $q\bar{q}$ and $B\bar{B}$ backgrounds. We veto J/ψ and $\psi(2S)$ mass regions and use them as control samples. Figures 3 and 4 show the m_{ES} and L_R distributions for $e^+ e^-$ modes in bin q_5 and for $\mu^+ \mu^-$ modes in bin q_1 , respectively.

We measure $d\mathcal{B}(B \rightarrow X_s \ell^+ \ell^-)/dq^2$ in six bins of $q^2 = m_{\ell\ell}^2$ and four bins of m_{X_s} defined in Table 2. We extract the signal in each bin from a two-dimensional fit to m_{ES} and L_R . Figure 5 shows the differential branching fraction as a function of q^2 (top) and m_{X_s} (bottom) [16].

Table 1: Exclusive modes used in the semi-inclusive $B \rightarrow X_s \ell^+ \ell^-$ analysis.

Mode	Mode
$B^0 \rightarrow K_S^0 \mu^+ \mu^-$	$B^+ \rightarrow K^+ \mu^+ \mu^-$
$B^0 \rightarrow K_S^0 e^+ e^-$	$B^+ \rightarrow K^+ e^+ e^-$
$B^0 \rightarrow K^{*0}(K_S^0 \pi^0) \mu^+ \mu^-$	$B^+ \rightarrow K^{*+}(K^+ \pi^0) \mu^+ \mu^-$
$B^0 \rightarrow K^{*0}(K^+ \pi^-) \mu^+ \mu^-$	$B^+ \rightarrow K^{*+}(K_S^0 \pi^+) \mu^+ \mu^-$
$B^0 \rightarrow K^{*0}(K_S^0 \pi^0) e^+ e^-$	$B^+ \rightarrow K^{*+}(K^+ \pi^0) e^+ e^-$
$B^0 \rightarrow K^{*0}(K^+ \pi^-) e^+ e^-$	$B^+ \rightarrow K^{*+}(K_S^0 \pi^+) e^+ e^-$
$B^0 \rightarrow K_S^0 \pi^+ \pi^- \mu^+ \mu^-$	$B^+ \rightarrow K_S^0 \pi^+ \pi^0 \mu^+ \mu^-$
$B^0 \rightarrow K^+ \pi^- \pi^0 \mu^+ \mu^-$	$B^+ \rightarrow K^+ \pi^+ \pi^- \mu^+ \mu^-$
$B^0 \rightarrow K_S^0 \pi^+ \pi^- e^+ e^-$	$B^+ \rightarrow K_S^0 \pi^+ \pi^0 e^+ e^-$
$B^0 \rightarrow K^+ \pi^- \pi^0 e^+ e^-$	$B^+ \rightarrow K^+ \pi^+ \pi^- e^+ e^-$

Table 2: Definition of the q^2 bins.

q^2 bin	q^2 range [GeV^2/c^4]	$m_{\ell\ell}$ range [GeV/c^2]	m_{X_s} bin
0	$1.0 < q^2 < 6.0$	$1.00 < m_{\ell\ell} < 2.45$	
1	$0.1 < q^2 < 2.0$	$0.32 < m_{\ell\ell} < 1.41$	1
2	$2.0 < q^2 < 4.3$	$1.41 < m_{\ell\ell} < 2.07$	2
3	$4.3 < q^2 < 8.1$	$2.07 < m_{\ell\ell} < 2.6$	3
4	$10.1 < q^2 < 12.9$	$3.18 < m_{\ell\ell} < 3.59$	4
5	$14.2 < q^2 < (m_B - m_K^*)^2$	$3.77 < m_{\ell\ell} < (m_B - m_K^*)$	

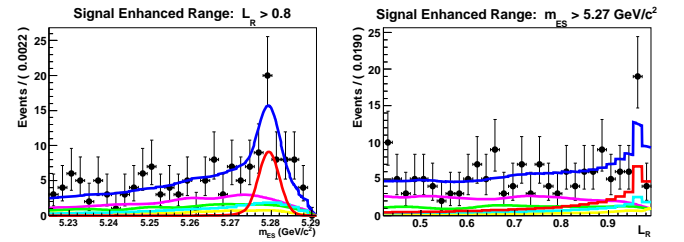


Figure 3: Distributions of m_{ES} (left) and likelihood ratio (right) for $B \rightarrow X_s e^+ e^-$ in q^2 bin q_5 showing data (points with error bars), the total fit (thick solid blue curves), signal component (red peaking curves), signal cross feed (cyan/light grey curves), $B\bar{B}$ background (magenta/dark grey smooth curve), $e^+ e^- \rightarrow q\bar{q}$ background (green/grey curves) and charmonium background (yellow/light grey curves).

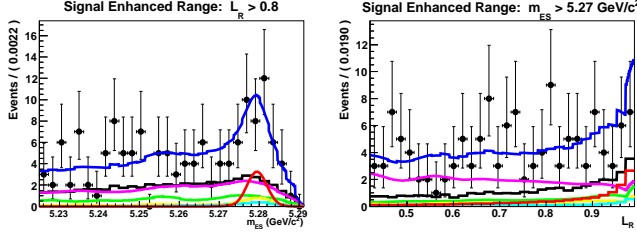


Figure 4: Distributions of m_{ES} (left) and likelihood ratio (right) for $B \rightarrow X_s \mu^+ \mu^-$ in q^2 bin q_1 showing data (points with error bars), the total fit (thick solid blue curves), signal component (red peaking curves), signal cross feed (cyan/grey curves), $B\bar{B}$ background (magenta/dark grey smooth curve), $e^+e^- \rightarrow q\bar{q}$ background (green/grey curves) and charmonium background (yellow/light grey curves)

Table 3 summarizes the differential branching fractions in the low and high q^2 regions in comparison to the SM predictions [17, 18, 19, 18, 20, 21, 22, 23, 24, 25, 26, 27]. In both regions of q^2 , the differential branching fraction is in good agreement with the SM prediction. These results supersede the previous *BABAR* measurements [28] and are in good agreement with the Belle results [29].

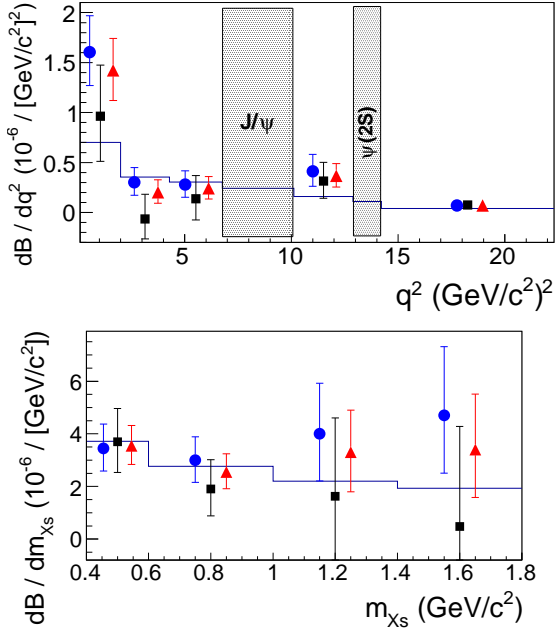


Figure 5: Differential branching fraction of $B \rightarrow X_s e^+ e^-$ (blue points), $B \rightarrow X_s \mu^+ \mu^-$ (black squares), and $B \rightarrow X_s \ell^+ \ell^-$ (red triangles) versus q^2 (top) and versus m_{X_s} (bottom) in comparison to the SM prediction (histogram). The grey-shaded bands show the J/ψ and $\psi(2S)$ vetoed regions.

Table 3: The $B \rightarrow X_s \ell^+ \ell^-$ branching fraction measurements in the low and high q^2 regions [16] in comparison to the SM prediction.

Mode	<i>BABAR</i> [10^{-6}]	SM [10^{-6}]
q^2 [GeV^2/c^4]	1 – 6	1 – 6
$B \rightarrow X_s \mu^+ \mu^-$	$0.66^{+0.82+0.30}_{-0.76-0.24} \pm 0.07$	1.59 ± 0.11
$B \rightarrow X_s e^+ e^-$	$1.93^{+0.47+0.21}_{-0.45-0.16} \pm 0.18$	1.64 ± 0.11
$B \rightarrow X_s \ell^+ \ell^-$	$1.60^{+0.41+0.17}_{-0.39-0.13} \pm 0.07$	
q^2 [GeV^2/c^4]	> 14.2	> 14.2
$B \rightarrow X_s \mu^+ \mu^-$	$0.60^{+0.31+0.05}_{-0.29-0.04} \pm 0.00$	$0.25^{+0.07}_{-0.06}$
$B \rightarrow X_s e^+ e^-$	$0.56^{+0.19+0.03}_{-0.18-0.03} \pm 0.00$	
$B \rightarrow X_s \ell^+ \ell^-$	$0.57^{+0.16+0.03}_{-0.15-0.02} \pm 0.00$	

The direct CP asymmetry is defined by:

$$\mathcal{A}_{CP} = \frac{\mathcal{B}(\bar{B} \rightarrow \bar{X}_s \ell^+ \ell^-) - \mathcal{B}(B \rightarrow X_s \ell^+ \ell^-)}{\mathcal{B}(\bar{B} \rightarrow \bar{X}_s \ell^+ \ell^-) + \mathcal{B}(B \rightarrow X_s \ell^+ \ell^-)}. \quad (2)$$

We use 14 self-tagging modes consisting of all B^+ modes and the B^0 modes with decays to a K^+ listed in Table 1 to measure $\mathcal{A}_{CP}(B \rightarrow X_s \ell^+ \ell^-)$ in five q^2 bins. Note that we have combined bins q_4 and q_5 due to low statistics. Figure 6 shows the CP asymmetry as a function of q^2 . The SM prediction of the CP asymmetry in the entire q^2 region is close to zero [30, 31, 32, 8]. In new physics models, however, \mathcal{A}_{CP} may be significantly enhanced [11, 33]. In the full range of q^2 we measure $\mathcal{A}_{CP} = 0.04 \pm 0.11 \pm 0.01$ [16], which is in good agreement with the SM prediction. The CP asymmetries in the five q^2 bins are also consistent with zero.

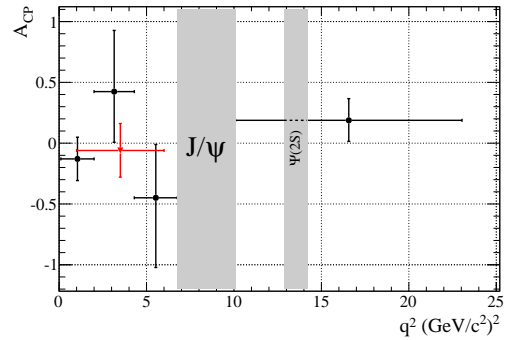


Figure 6: The CP asymmetry as a function of q^2 . The grey-shaded bands show the J/ψ and $\psi(2S)$ vetoed regions.

3. Study of $B \rightarrow X_s \gamma$

In the SM, the $B \rightarrow X_s \gamma$ branching fraction is calculated in next-to-next leading order (4 loops) yielding

$$\mathcal{B}(B \rightarrow X_s \gamma) = (3.15 \pm 0.23) \times 10^{-4} \quad (3)$$

for photon energies $E_\gamma > 1.6$ GeV [34, 35].

To extract the $B \rightarrow X_s \gamma$ signal experimentally from $e^+e^- \rightarrow B\bar{B}$ and $e^+e^- \rightarrow q\bar{q}$ backgrounds, we use two very different strategies. The first strategy consists of a semi-inclusive approach in which we sum over 38 exclusive $B \rightarrow X_s \gamma$ final states with $1K^\pm (\leq 1K_s^0)$ or $3K^\pm, \leq 4\pi (\leq 2\pi^0)$, and $\leq 1\eta$. We use no tagging of the other B meson. We need to model the missing modes. Due to large backgrounds, we select events with a minimum photon energy of $E_\gamma > 1.9$ GeV and then extrapolate the branching fraction to photon energies $E_\gamma > 1.6$ GeV. With this approach, we measure the branching fraction, CP asymmetry and the difference in CP asymmetries between charged and neutral B decays using $471 \times 10^6 B\bar{B}$ events [36].

The second strategy is a fully inclusive approach. To suppress backgrounds from $B\bar{B}$ and $q\bar{q}$ decays, we impose stringent constraints on isolated photons to remove clusters that may have originated from π^0 and η decays. We use a semileptonic tag of the other B meson and require a minimum photon energy of $E_\gamma > 1.8$ GeV but impose no requirements on the hadronic mass system. Using $383 \times 10^6 B\bar{B}$ events, we measure the $B \rightarrow X_s \gamma$ branching fraction measurement and the CP asymmetry for $B \rightarrow X_{s+d} \gamma$ [37, 38].

Table 4 summarizes our $B \rightarrow X_s \gamma$ branching fraction measurements of the semi-inclusive and fully inclusive methods [36, 37, 38]. Figure 7 shows the *BABAR* results extrapolated to a minimum photon energy of 1.6 GeV in comparison to results from Belle [40, 41, 42], CLEO [43] and the SM prediction [34, 35]. Our results are in good agreement with those of the other experiments as well as the SM prediction.

For the semi-inclusive method, the direct CP asymmetry is defined by:

$$\mathcal{A}_{CP}(X_s \gamma) = \frac{\mathcal{B}(\bar{B} \rightarrow \bar{X}_s \gamma) - \mathcal{B}(B \rightarrow X_s \gamma)}{\mathcal{B}(\bar{B} \rightarrow \bar{X}_s \gamma) + \mathcal{B}(B \rightarrow X_s \gamma)}. \quad (4)$$

The SM prediction yields $-0.6\% < \mathcal{A}_{CP}(B \rightarrow X_s \gamma) < 2.8\%$ [45, 46]. Using 16 self-tagging exclusive modes and $471 \times 10^6 B\bar{B}$ events, we measure $\mathcal{A}_{CP}(B \rightarrow X_s \gamma) = (1.7 \pm 1.9_{stat} \pm 1.0_{sys})\%$ [47]. This supersedes the old *BABAR* measurement [48]. We further measure the CP asymmetry difference between charged and neutral B decays:

$$\Delta \mathcal{A}_{CP} = \mathcal{A}_{CP}(B^+ \rightarrow X_s^+ \gamma) - \mathcal{A}_{CP}(B^0 \rightarrow X_s^0 \gamma), \quad (5)$$

Table 4: Our measurements of $\mathcal{B}(B \rightarrow X_s \gamma)$ from the semi-inclusive [36] and fully-inclusive [37] analyses and their extrapolations to $E_\gamma > 1.6$ GeV. The first uncertainty is statistical, the second is systematic and the third is from model dependence and extrapolation to 1.6 GeV.

method	$E_\gamma >$	$\mathcal{B}(B \rightarrow X_s \gamma) [10^{-4}]$
semi-exclusive	1.9 GeV	$3.29 \pm 0.19 \pm 0.48$
	1.6 GeV	$3.52 \pm 0.20 \pm 0.51 \pm 0.04$
inclusive	1.8 GeV	$3.21 \pm 0.15 \pm 0.29 \pm 0.08$
	1.6 GeV	$3.31 \pm 0.16 \pm 0.30 \pm 0.10$

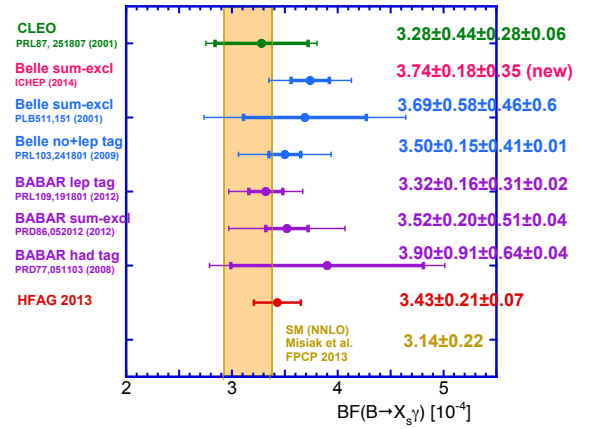


Figure 7: Summary of $\mathcal{B}(B \rightarrow X_s \gamma)$ measurements from BABAR [36, 37, 38, 39], Belle [40, 41, 42], CLEO [43] and the HFAG average [44] in comparison to the SM prediction [34, 35] after extrapolation to $E_\gamma > 1.6$ GeV.

which depends on the Wilson coefficients C_7^{eff} and C_8^{eff} :

$$\Delta \mathcal{A}_{CP} = 4\pi^2 \alpha_s \frac{\bar{\Lambda}_{78}}{m_b} \text{Im} \frac{C_8^{\text{eff}}}{C_7^{\text{eff}}} \approx 0.12 \frac{\bar{\Lambda}_{78}}{100 \text{ MeV}} \text{Im} \frac{C_8^{\text{eff}}}{C_7^{\text{eff}}} \quad (6)$$

where the scale parameter $\bar{\Lambda}_{78}$ is constrained by $17 \text{ MeV} < \bar{\Lambda}_{78} < 190 \text{ MeV}$. In the SM, C_7^{eff} and C_8^{eff} are real so that $\Delta \mathcal{A}_{CP}$ vanishes. However in new physics parts yielding a non-vanishing $\Delta \mathcal{A}_{CP}$.

From a simultaneous fit to charged and neutral B decays, we measure $\Delta \mathcal{A}_{CP}(B \rightarrow X_s \gamma) = (5.0 \pm 3.9_{stat} \pm 1.5_{sys})\%$ from which we set an upper and lower limit at 90% CL on $\text{Im}(C_8^{\text{eff}}/C_7^{\text{eff}})$ [47]:

$$-1.64 < \text{Im} \frac{C_8^{\text{eff}}}{C_7^{\text{eff}}} < 6.52 \text{ at } 90\% \text{ CL}. \quad (7)$$

This is the first $\Delta \mathcal{A}_{CP}$ measurements and the first constraint on $\text{Im}(C_8^{\text{eff}}/C_7^{\text{eff}})$. Figure 8 (top) shows the $\Delta \chi^2$ of

the fit as a function of $\text{Im}(C_8^{\text{eff}}/C_7^{\text{eff}})$. The shape of $\Delta\chi^2$ as a function of $\text{Im}(C_8^{\text{eff}}/C_7^{\text{eff}})$ is not parabolic indicating that the likelihood has a non-Gaussian shape. The reason is that $\Delta\chi^2$ is determined from all possible values of $\bar{\Lambda}_{78}$. In the region $\sim 0.2 < \text{Im}(C_8^{\text{eff}}/C_7^{\text{eff}}) < \sim 2.6$ a change in $\text{Im}(C_8^{\text{eff}}/C_7^{\text{eff}})$ $\Delta\chi^2$ can be compensated by a change in $\bar{\Lambda}_{78}$ leaving $\Delta\chi^2$ unchanged. For positive values larger (smaller) than 2.6 (0.2), $\Delta\chi^2$ increases slowly (rapidly), since $\bar{\Lambda}_{78}$ remains nearly constant at the minimum value (increases rapidly). For negative $\text{Im}(C_8^{\text{eff}}/C_7^{\text{eff}})$ values, $\bar{\Lambda}_{78}$ starts to decrease again, which leads to a change in the $\Delta\chi^2$ shape. Figure 8 (bottom) shows $\bar{\Lambda}_{78}$ as a function of $\text{Im}(C_8^{\text{eff}}/C_7^{\text{eff}})$.

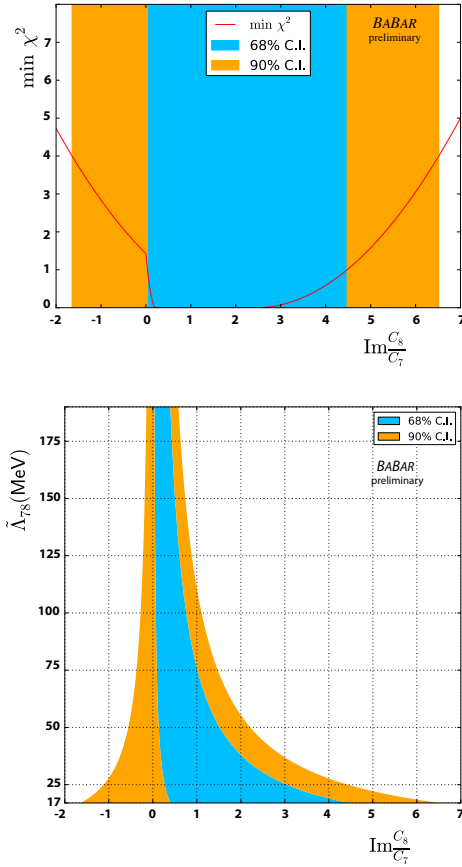


Figure 8: The $\Delta\chi^2$ function versus $\text{Im}(C_8^{\text{eff}}/C_7^{\text{eff}})$ (top) and the dependence of $\bar{\Lambda}_{78}$ on $\text{Im}(C_8^{\text{eff}}/C_7^{\text{eff}})$ (bottom). The blue dark-shaded (orange light-shaded) regions show the 68% (90%) CL intervals.

In the fully-inclusive analysis, the $B \rightarrow X_d$ decay cannot be separated from the $B \rightarrow X_s$ decay and we measure:

$$\mathcal{A}_{CP}(X_{s+d}\gamma) = \frac{\mathcal{B}(\bar{B} \rightarrow \bar{X}_{s+d}\gamma) - \mathcal{B}(B \rightarrow X_{s+d}\gamma)}{\mathcal{B}(\bar{B} \rightarrow \bar{X}_{s+d}\gamma) + \mathcal{B}(B \rightarrow X_{s+d}\gamma)}. \quad (8)$$

In the SM, $\mathcal{A}_{CP}(B \rightarrow X_{s+d}\gamma)$ is zero [49]. From the charge of the B and \bar{B} , we determine the CP asymmetry. Using 383×10^6 $B\bar{B}$ events, we measure $\mathcal{A}_{CP}(B \rightarrow X_{s+d}\gamma) = (5.7 \pm 6.0 \pm 1.8)\%$, which is consistent with the SM prediction [49]. Figure 9 shows a summary of all CP asymmetry measurements in comparison to the SM predictions.

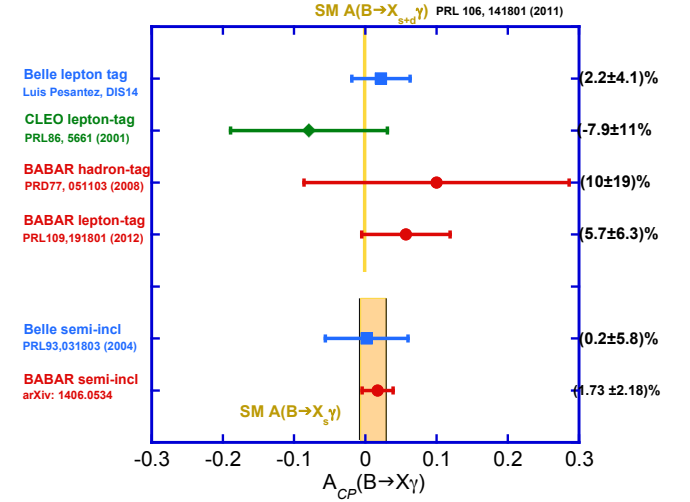


Figure 9: Summary of \mathcal{A}_{CP} measurements for $B \rightarrow X_s\gamma$ from semi-inclusive analyses (*BABAR* [47], Belle [50]) and for $B \rightarrow X_{s+d}\gamma$ from fully inclusive analyses (*BABAR* [37, 38, 39], CLEO [51], Belle [52] and the HFAG average [44] in comparison to the SM prediction for $B \rightarrow X_s\gamma$ [45, 46, 49].

4. Conclusion

We performed the first \mathcal{A}_{CP} measurement in five q^2 bins in semi-inclusive $B \rightarrow X_s\ell^+\ell^-$ decays and updated the differential branching fraction. The $B \rightarrow X_s\ell^+\ell^-$ partial branching fractions and CP asymmetries are in good agreement with the SM predictions. Our \mathcal{A}_{CP} measurement in the semi-inclusive $B \rightarrow X_s\gamma$ decay is the most precise CP asymmetry measurement. The $\Delta\mathcal{A}_{CP}(B \rightarrow X_s\gamma)$ result yields first constraint on $\text{Im}(C_8^e/C_7^e)$. The $B \rightarrow X_s\gamma$ branching fractions and CP asymmetries are both in good agreement with the SM predictions. New progress on these inclusive decays will come from Belle II. For the $B \rightarrow X_s\gamma$ and $B \rightarrow X_s\ell^+\ell^-$ semi-inclusive decays, we expect precision measurements. For the inclusive $B \rightarrow X_s\gamma$ and $B \rightarrow X_s\ell^+\ell^-$ decays, we expect new possibilities by tagging the other \bar{B} meson via full B reconstruction.

5. Acknowledgments

This work was supported by the Norwegian Research Council. I would like to thank members of the *BABAR* collaboration for giving me the opportunity to present these results. In particular, I would like to thank Doug Roberts, Liang Sun and David Hitlin for their fruitful suggestions.

References

- [1] K. G. Wilson, Phys. Rev. **179**, 1499 (1969).
- [2] K. G. Wilson and J. B. Kogut, Phys. Rept. **12**, 75 (1974).
- [3] N. Isgur, D. Scora, B. Grinstein and M. B. Wise, Phys. Rev. D **39**, 799 (1989).
- [4] N. Isgur and M. B. Wise, Phys. Lett. B **232**, 113 (1989).
- [5] H. Georgi, Phys. Lett. B **240**, 447 (1990).
- [6] B. Grinstein and D. Pirjol, Phys. Rev. D **70**, 114005 (2004) [hep-ph/0404250].
- [7] G. Buchalla, A. J. Buras and M. E. Lautenbacher, Rev. Mod. Phys. **68**, 1125 (1996) [hep-ph/9512380].
- [8] W. Altmannshofer, P. Ball, A. Bharucha, A. J. Buras, D. M. Straub and M. Wick, JHEP **0901**, 019 (2009) [arXiv:0811.1214 [hep-ph]].
- [9] A. Ali, E. Lunghi, C. Greub and G. Hiller, Phys. Rev. D **66**, 034002 (2002) [hep-ph/0112300].
- [10] K. S. M. Lee and F. J. Tackmann, Phys. Rev. D **79**, 114021 (2009) [arXiv:0812.0001 [hep-ph]].
- [11] A. Soni, A. K. Alok, A. Giri, R. Mohanta and S. Nandi, Phys. Rev. D **82**, 033009 (2010) [arXiv:1002.0595 [hep-ph]].
- [12] S. Oh and J. Tandean, Phys. Rev. D **83**, 095006 (2011) [arXiv:1102.1680 [hep-ph]].
- [13] S. Descotes-Genon, D. Ghosh, J. Matias and M. Ramon, JHEP **1106**, 099 (2011) [arXiv:1104.3342 [hep-ph]].
- [14] W. Altmannshofer, P. Paradisi and D. M. Straub, JHEP **1204**, 008 (2012) [arXiv:1111.1257 [hep-ph]].
- [15] N. Kosnik, Phys. Rev. D **86**, 055004 (2012) [arXiv:1206.2970 [hep-ph]].
- [16] J. P. Lees *et al.* [BaBar Collaboration], Phys. Rev. Lett. **112**, 211802 (2014) [arXiv:1312.5364 [hep-ex]].
- [17] H. H. Asatryan, H. M. Asatrian, C. Greub and M. Walker, Phys. Rev. D **65**, 074004 (2002) [hep-ph/0109140].
- [18] H. H. Asatryan, H. M. Asatrian, C. Greub and M. Walker, Phys. Rev. D **66**, 034009 (2002) [hep-ph/0204341].
- [19] A. Ghinculov, T. Hurth, G. Isidori and Y. P. Yao, Nucl. Phys. B **648**, 254 (2003) [hep-ph/0208088].
- [20] P. Gambino, M. Gorbahn and U. Haisch, Nucl. Phys. B **673**, 238 (2003) [hep-ph/0306079].
- [21] A. Ghinculov, T. Hurth, G. Isidori and Y. P. Yao, Eur. Phys. J. C **33**, S288 (2004) [hep-ph/0310187].
- [22] C. Bobeth, P. Gambino, M. Gorbahn and U. Haisch, JHEP **0404**, 071 (2004) [hep-ph/0312090].
- [23] A. Ghinculov, T. Hurth, G. Isidori and Y. P. Yao, Nucl. Phys. B **685**, 351 (2004) [hep-ph/0312128].
- [24] C. Greub, V. Pilipp and C. Schubach, JHEP **0812**, 040 (2008) [arXiv:0810.4077 [hep-ph]].
- [25] T. Huber, T. Hurth and E. Lunghi, Nucl. Phys. B **802**, 40 (2008) [arXiv:0712.3009 [hep-ph]].
- [26] T. Huber, E. Lunghi, M. Misiak and D. Wyler, Nucl. Phys. B **740**, 105 (2006) [hep-ph/0512066].
- [27] M. Beneke, G. Buchalla, M. Neubert and C. T. Sachrajda, Eur. Phys. J. C **61**, 439 (2009) [arXiv:0902.4446 [hep-ph]].
- [28] B. Aubert *et al.* [BaBar Collaboration], Phys. Rev. Lett. **93**, 081802 (2004) [hep-ex/0404006].
- [29] M. Iwasaki *et al.* [Belle Collaboration], Phys. Rev. D **72**, 092005 (2005) [hep-ex/0503044].
- [30] D. S. Du and M. Z. Yang, Phys. Rev. D **54**, 882 (1996) [hep-ph/9510267].
- [31] A. Ali and G. Hiller, Eur. Phys. J. C **8**, 619 (1999) [hep-ph/9812267].
- [32] C. Bobeth, G. Hiller and G. Piranishvili, JHEP **0807**, 106 (2008) [arXiv:0805.2525 [hep-ph]].
- [33] A. K. Alok, A. Dighe and S. Ray, Phys. Rev. D **79**, 034017 (2009) [arXiv:0811.1186 [hep-ph]].
- [34] M. Misiak, H. M. Asatrian, K. Bieri, M. Czakon, A. Czarnecki, T. Ewerth, A. Ferroglia and P. Gambino *et al.*, Phys. Rev. Lett. **98**, 022002 (2007) [hep-ph/0609232].
- [35] M. Misiak and M. Steinhauser, Nucl. Phys. B **764**, 62 (2007) [hep-ph/0609241].
- [36] J. P. Lees *et al.* [BaBar Collaboration], Phys. Rev. D **86**, 052012 (2012) [arXiv:1207.2520 [hep-ex]].
- [37] J. P. Lees *et al.* [BaBar Collaboration], Phys. Rev. Lett. **109**, 191801 (2012) [arXiv:1207.2690 [hep-ex]].
- [38] J. P. Lees *et al.* [BaBar Collaboration], Phys. Rev. D **86**, 112008 (2012) [arXiv:1207.5772 [hep-ex]].
- [39] B. Aubert *et al.* [BaBar Collaboration], Phys. Rev. D **77**, 051103 (2008) [arXiv:0711.4889 [hep-ex]].
- [40] K. Abe *et al.* [Belle Collaboration], Phys. Lett. B **511**, 151 (2001) [hep-ex/0103042].
- [41] A. Limosani *et al.* [Belle Collaboration], Phys. Rev. Lett. **103**, 241801 (2009) [arXiv:0907.1384 [hep-ex]].
- [42] T. Saito *et al.* [Belle Collaboration], Talk at Moriond Electroweak 2014.
- [43] S. Chen *et al.* [CLEO Collaboration], Phys. Rev. Lett. **87**, 251807 (2001) [hep-ex/0108032].
- [44] D. Asner *et al.* [Heavy Flavor Averaging Group Collaboration], arXiv:1010.1589 [hep-ex].
- [45] A. L. Kagan and M. Neubert, Phys. Rev. D **58**, 094012 (1998) [hep-ph/9803368].
- [46] M. Benzke, S. J. Lee, M. Neubert and G. Paz, Phys. Rev. Lett. **106**, 141801 (2011) [arXiv:1012.3167 [hep-ph]].
- [47] J. P. Lees *et al.* [BaBar Collaboration], arXiv:1406.0534 [hep-ex].
- [48] B. Aubert *et al.* [BaBar Collaboration], Phys. Rev. Lett. **101**, 171804 (2008) [arXiv:0805.4796 [hep-ex]].
- [49] T. Hurth, E. Lunghi and W. Porod, Nucl. Phys. B **704**, 56 (2005) [hep-ph/0312260].
- [50] S. Nishida *et al.* [Belle Collaboration], Phys. Rev. Lett. **93**, 031803 (2004) [hep-ex/0308038].
- [51] T. E. Coan *et al.* [CLEO Collaboration], Phys. Rev. Lett. **86**, 5661 (2001) [hep-ex/0010075].
- [52] L. Pesantez *et al.* [Belle Collaboration], talk at DIS14, arXiv:1406.6356 [hep-ex].